Fermi Surface Restructuring in the Repulsive Fermi-Hubbard Model

Author: Ian Osborne

Project Advisor:
Dr. Nandini Trivedi

Undergraduate Research Thesis

Presented in Partial Fulfillment of the Requirements for graduation with Research Distinction in Physics in the undergraduate colleges of The Ohio State University

March, 2020

The Ohio State University

Abstract

We take an in depth look into the celebrated Fermi-Hubbard model for strongly interacting fermions, beginning with a two-site exact diagonalization demonstration of the Mott ground state. We continue with measurements of compressibility and susceptibility using Determinantal Quantum Monte Carlo (DQMC) methods on a larger square lattice (6×6) over the parameter space of interaction strength U/t and doping, controlled by the chemical potential, μ/t. We construct the Fermi surface for a 16×16 cluster size using the retarded Green's function and the single particle spectral function (derived from the Green's function using an analytic continuation procedure) and find conclusive evidence of Fermi surface restructuring (FSR) as a result of strong interactions freezing out states from contributing to the Luttinger count, n, at intermediate temperatures, $T = t/2$. FSR is found for strongly interacting, doped systems for dopings $p \lesssim 0.2$. This phase is dubbed the Luttinger's rule breaking (LB) phase, and we provide a discussion of the consequences of the deviation from Luttinger's theorem. We strongly suggest a topological nature underlying the restructuring of the Fermi surface by eliminating competing ordering in spin or charge channels.

1 Introduction

The Hubbard Model is the paradigmatic model for understanding Mott insulators, strongly correlated metals, and high Tc superconductors [2]. Ever since the 60s, when it was first proposed, the Hubbard model has remarkably proven to predict emergent magnetic phenomenon in strongly interacting systems in spite of its incredible simplicity, and has remained a key tool in our understanding of some of the most elusive questions in condensed matter physics.

The relatively new realization of the Hubbard model goes beyond quantum materials to cold atoms trapped in an optical lattice. This platform has provided the phase diagram of the Hubbard model in any dimension due to the ease of tuning its parameters using optical lattices. Spin sensitive Bragg scattering measurements on these trapped, cold atoms find the anti-ferromagnetic correlations characteristic of the Mott phase, [3] elevating the Hubbard model as a quantum emulator of strongly interacting systems. These experiments have provided insight into fields such as quantum magnetism, exotic superconductors, quantum criticality, topological materials, disordered insulators, and entanglement, and has allowed us to explore new regimes like the strange metal and canted anti-ferromagnetism phase of the magnetized Hubbard model.[4] Each of these observations closely agree with numerical calculations which serves to increase the confidence of the Hubbard model to represent physics found in strongly correlated materials.

The Hubbard model in a one dimensional chain is exactly solvable,[5] and is otherwise well understood from numerical calculations. Much of the remaining physics resides in the two-dimensional Hubbard model, which is used to understand the mechanism of high-Tc superconductivity in the cuprates [6, 7], given that the model qualitatively exhibits d-wave superconductivity itself.[8]

The field of high-TC superconducting cuprates is another arena for the physics of the Hubbard model to enhance our understanding given the strongly interacting nature of the charge carriers that lead to Cooper pairing and resistanceless

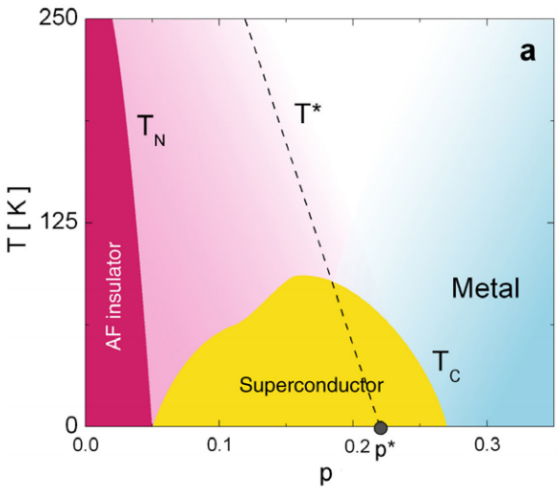

Figure 1: The phase diagram of a high-TC superconductor in terms of temperature and hole doping, p. At zero doping, strong interactions inside the cuprates drive a Mott phase with anti-ferromagnetic correlations. In the large doping limit, $p > 0.3$, the system behaves as a Fermi-liquid. Below a critical temperature, T_C, and centered around a critical doping, p^*, a superconducting phase emerges where charge transports without resistance. Increasing the temperature above T_C but below T^* one finds the anomalous pseudogap phase, which has been directly linked to the superconducting phase, and has consistently shown evidence of Fermi surface reconstruction.[1]

transport. The phase diagram of hole-doped cuprates exhibits familiar phases to the standard Hubbard model such as an antiferromagnetic/Mott phase at zero doping and a metallic phase at larger doping (see Fig 1). A key feature of the cuprate phase diagram which is imperative to the understanding of the superconducting phase is the pseudogap phase, which occurs below a doping p^* and below the doping dependent critical temperature T^*. The importance of the normal-state pseudogap phase is emphasized by the ubiquity of its presence among all high-TC superconductors, as well as the evidence that the pseudogap gives rise to the superconducting gap.[9] Large magnetic fields are used to suppress superconductivity below the critical temperature T_C to allow the study of the pseudogap phase at low-T. These studies find that a range of doping in the pseudogap phase feature reconstructed Fermi surfaces to form small electron-like pockets on the border of what was originally the large hole-like Fermi surface. This reconstruction has been attributed to stripe order which is a state with both charge and spin modulations.[1]

Recently, however, Hall measurements on magnetically suppressed cuprates in the pseudogap phase have concluded the existence of a distinct Fermi surface restructuring event outside of the doping regime for charge density wave ordering, which remains unexplained.[10] Furthermore, angle-resolved photoemission (ARPES) measurements on electron doped cuprates conclude Fermi surface reconstruction can occur in the absence of long-ranged antiferromagnetic order.[11] In this study, we present a practical look at the Fermi-Hubbard model and tackle the question of how the Fermi surface transforms in the Mott limit, where particle-particle interactions are strong enough to drive the metal-insulator phase transition. In the Mott limit does the Fermi surface simply vanish gradually? Does the Fermi surface count all of the electrons, as is necessitated by Luttinger's theorem[12] or are states being frozen out due to interactions? Is the Fermi surface large or small? If small, then where is the critical doping for the transition and can we assign some underlying order that is causing the restructuring of the Fermi surface? In other words, is the restructuring of the Fermi surface due to some competing order or is there topological or hidden order that is the cause?

Our aim is to extract the underlying Fermi surface and show its transition across the metal-insulator phase transition. We use several methods for obtaining different interpretations of the Fermi surface, however all methods are derived from the imaginary time Green's function, $G_{\mathbf{k}}(\tau)$, which is obtained from determinantal quantum Monte Carlo simulations as a function of doping. Remarkably, we find evidence of Fermi surface restructuring in the absence of any competing order.

2 The Hubbard Hamiltonian

A simple metal, characterized by free moving charges, is modeled using the tight binding Hamiltonian, which assumes an electron's wave-function can be written as a linear combination of atomic orbitals. Taking advantage of the formalisms of second quantization, the tight binding Hamiltonian is

$$\mathcal{H}_{TB} = -\sum_{i,j,\sigma} \hat{c}^{\dagger}_{i,\sigma} t_{ij} \hat{c}_{j,\sigma} + h.c. \quad -\sum_{i,\sigma} \mu_i \hat{n}_{i,\sigma} \tag{1}$$

Where i and j denote distinct lattice coordinates and σ is the spin flavor. In the context of electrons, σ ranges from $\sigma \in \{+1/2, -1/2\}$ or $\{\uparrow, \downarrow\}$. The operator $\hat{c}_{i,\sigma}$ and its hermitian conjugate (h.c.) $\hat{c}^{\dagger}_{i,\sigma}$ annihilate and create a particle on site i with spin flavor σ respectively. These operators obey different commutation relations depending on if the particles are fermions or bosons. Since we are studying Fermi surfaces and modeling metals, we use fermionic charge carriers which obey the following anti-commutation rules:

$$\{\hat{c}^{\dagger}_{i,\sigma}, \hat{c}^{\dagger}_{j,\sigma'}\} = 0 \quad \{\hat{c}_{i,\sigma}, \hat{c}_{j,\sigma'}\} = 0 \quad \{\hat{c}_{i,\sigma}, \hat{c}^{\dagger}_{j,\sigma'}\} = \delta_{i,j}\delta_{\sigma,\sigma'} \tag{2}$$

The first term in equation 1 is the "hopping" term because the process of destroying a particle on one site and creating a particle on another describes the hopping, or phenomenologically the tunneling, of a particle from one site to the next. $t_{ij} = t_{ji}$ is the hopping amplitude from site i to site j and is related to the likelihood that a tunneling event occurs. The second term merely sums the particles on the lattice as $\hat{n}_{i,\sigma} = \hat{c}^{\dagger}_{i,\sigma}\hat{c}_{i,\sigma}$ is the number operator. μ_i is the local chemical potential.

Take the hopping term to be zero for non-adjacent sites because the atomic orbital wave-function drops off exponentially from their own nucleus. Next, assume that each atom is identical such that the chemical potential for each atom is a constant. These approximations simplify the Hamiltonian with a Fourier transform: define the momentum annihilation operator by the Fourier transform of the on-site annihilation operator:

$$\hat{c}_{\mathbf{k}} = \frac{1}{\sqrt{N}} \sum_{\mathbf{j}}^{N} e^{i\mathbf{j}\cdot\mathbf{k}} \hat{c}_{\mathbf{j}} \qquad \hat{c}_{\mathbf{k}}^{\dagger} = \frac{1}{\sqrt{N}} \sum_{\mathbf{j}}^{N} e^{-i\mathbf{j}\cdot\mathbf{k}} \hat{c}_{\mathbf{j}}^{\dagger} \tag{3}$$

Using these momentum space operators and noting that $\hat{n}_k \equiv \hat{c}_k^{\dagger}\hat{c}_k$ the one dimensional tight binding chain becomes

$$\mathcal{H} = \sum_{k} (-2t\cos(k) - \mu)\hat{n}_k \tag{4}$$

Where k ranges from $-\pi$ to π in discrete steps of $2\pi/N$. Fig 2 demonstrates what this dispersion looks like for a one dimensional tight binding chain with periodic boundary conditions.

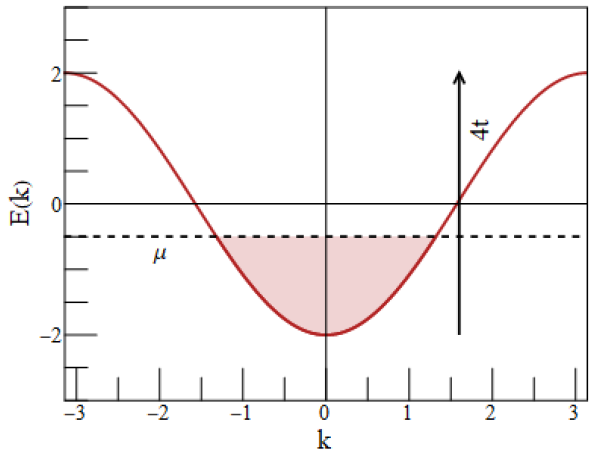

Figure 2: The band structure for a one dimensional tight binding chain where states are filled based on the chemical potential at zero temperature. The band width is 4t and the units of E are t.

On a square lattice the Hamiltonian is

$$\mathcal{H} = \sum_{\mathbf{k}} (-2t\cos(k_x) - 2t\cos(k_y) - \mu)\hat{n}_{\mathbf{k}} \tag{5}$$

and so on for three dimensional tight binding models. The dispersion relation for the two dimensional tight binding model is integral to this study, thus we show it as a contour plot over the Brillouin zone in Fig 3. Note that every contour is of constant energy, implying it is a distinct Fermi surface for a specific doping of the lattice. The Lifshitz transition occurs at $n = 1$, corresponding to the diamond contour. This is the boundary where the Fermi surface changes from a hole-like Fermi surface for $n > 1$ to an electron-like surface for $n < 1$.

The tight binding model is the basis for the band theory of metals, however equation 1 does not account for the Coulomb interaction between electrons, which turns out to be a significant factor in materials. The Hubbard term ameliorates this by assigning an energy cost of U whenever two electrons exist on the same site.

$$\mathcal{H}_H = U \sum_{i} \hat{n}_{\uparrow,i}\hat{n}_{\downarrow,i} \tag{6}$$

The value of U is called the interaction potential, and is usually contrasted as a fraction of the hopping potential, t. Note that since each number operator contains two annihilation or creation operators, the Hubbard term is no longer quadratic like the tight binding model. In fact, it is quartic, and impossible to solve analytically for arbitrarily large systems as is the case for the tight binding model. The Hubbard Hamiltonian is thus

$$\mathcal{H} = \mathcal{H}_{TB} + \mathcal{H}_H \tag{7}$$

$$= -t \sum_{\langle i,j\rangle,\sigma} \hat{c}_{i,\sigma}^{\dagger}\hat{c}_{j,\sigma} + h.c. \; - \mu \sum_{i,\sigma} \hat{n}_{i,\sigma} \; + U \sum_{i} \hat{n}_{\uparrow,i}\hat{n}_{\downarrow,i} \tag{8}$$

Where $\langle i, j\rangle$ is short hand for nearest neighbor sites. We can make a simple transformation where $\mu \to \mu + U/2$ which ensures that when the chemical potential is zero the lattice is half-filled (one particle per site).

$$\mathcal{H} = -t \sum_{\langle i,j\rangle,\sigma} \hat{c}^\dagger_{i,\sigma}\hat{c}_{j,\sigma} + h.c. \; + U \sum_i (\hat{n}_{\uparrow,i} - \frac{1}{2})(\hat{n}_{\downarrow,i} - \frac{1}{2}) \; - \mu \sum_{i,\sigma} \hat{n}_{i,\sigma} \tag{9}$$

An important feature about equation 9 is that on a bipartite lattice (one that can be divided into a sublattice of "A" sites and a sublattice of "B" sites where all sites in A are only adjacent to sites in B and vice-versa) this Hamiltonian is particle-hole symmetric around $\mu = 0$.

Specifically, a substitution of particle annihilation operators with hole creation operators yields the exact same Hamiltonian.

$$\hat{c}_{i,\sigma} \to (-1)^i \; \hat{d}^\dagger_{i,\sigma} \quad \hat{c}^\dagger_{i,\sigma} \to (-1)^i \; \hat{d}_{i,\sigma} \tag{10}$$

The Fourier transform of the Hubbard term is

$$\mathcal{H}_H = U \sum_{k,q,p} \hat{c}^\dagger_k \hat{c}^\dagger_q \hat{c}_p \hat{c}_{k+q-p} \tag{11}$$

which scatters particles in k-space. At $T = 0$ scattering will kick particles from inside the Fermi surface to outside, blurring the boundary itself. Nevertheless, a finite step size in the density, $0 < Z \leq 1$ should persist at the Fermi surface according to Fermi liquid theory.

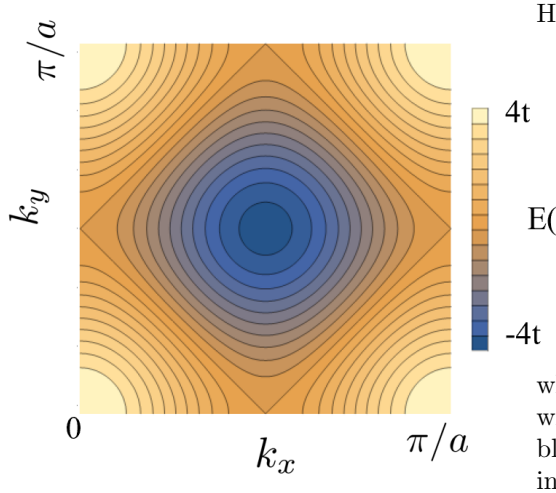

Figure 3: The dispersion relation for a two dimensional tight binding model over the Brillouin zone. Note that each of these contours is a Fermi surface of a given doping (which is set by μ). The Fermi surface is a diamond when the system is half-filled at $\mu = 0$.

3 Two Site Example

Often times, an analytic solution on a small scale can provide the much needed intuition for large scale behavior, where analytic solutions are intractable. With this attitude, let's explore the two site exact diagonalization Fermi-Hubbard model. The size of our basis is $4^2 = 16$ since there are 4 single site arrangements of particles:

$$\{|0\rangle, |\uparrow\rangle, |\downarrow\rangle, |\uparrow\downarrow\rangle\} \tag{12}$$

The number operators $\hat{n}_\uparrow = \sum_i \hat{n}_{\uparrow,i}$ and $\hat{n}_\downarrow = \sum_i \hat{n}_{\downarrow,i}$ both commute with the Hamiltonian, implying conservation of particle number and total spin. This let's us solve much smaller matrices than 16×16 by block diagonalizing by both particle and total spin.

The trivial cases, where only one state exists in its block are as followed with the corresponding energies eigenvalues:

$$\mathcal{H}|0_1 0_2\rangle = U/2|0_1 0_2\rangle \tag{13}$$
$$\mathcal{H}|\uparrow_1\uparrow_2\rangle = (-2\mu - U/2)|\uparrow_1\uparrow_2\rangle \tag{14}$$
$$\mathcal{H}|\downarrow_1\downarrow_2\rangle = (-2\mu - U/2)\,|\downarrow_1\downarrow_2\rangle \tag{15}$$
$$\mathcal{H}|\uparrow\downarrow_1\uparrow\downarrow_2\rangle = (-4\mu + U/2)\,|\uparrow\downarrow_1\uparrow\downarrow_2\rangle \tag{16}$$
$$\tag{17}$$

Remember that our particle hole symmetric Hamiltonian (eq.9) adds an interaction cost to the empty sites equal to the energy cost of a doubly occupied site.

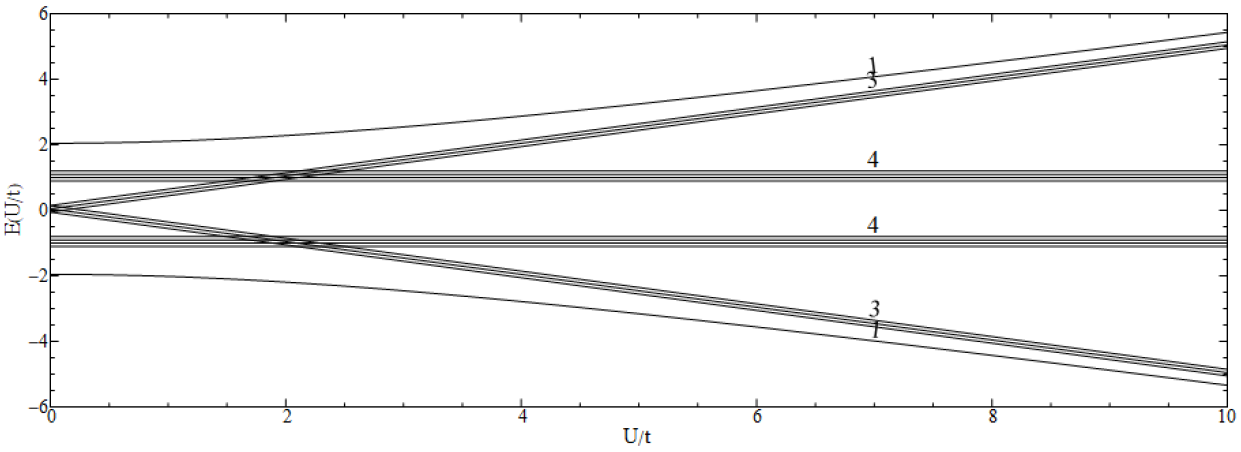

Figure 4: The spectrum of the two site Fermi-Hubbard model as a function U/t with $\mu = 0$ and $t = 1$. The numbers show the degeneracy of each band. For very large U/t the lower two bands approach the same value, with the gap between the singlet ground state and the triplet state calculated perturbatively to be $4t^2/U$.

After the trivial cases are calculated, we are left with four 2×2 blocks with one and three particles, and a $4\times$ 4 block of two particles.

$$|\uparrow_1 0_2\rangle \quad |0_1 \uparrow_2\rangle \tag{18}$$

$$\begin{pmatrix} -\mu & -t \\ -t & -\mu \end{pmatrix} \tag{19}$$

$$\implies \mathcal{H}\left(|\uparrow_1 0_2\rangle + |0_1 \uparrow_2\rangle\right) = (-\mu - t)\left(|\uparrow_1 0_2\rangle + |0_1 \uparrow_2\rangle\right) \tag{20}$$

$$\mathcal{H}\left(|\uparrow_1 0_2\rangle - |0_1 \uparrow_2\rangle\right) = (-\mu + t)\left(|\uparrow_1 0_2\rangle - |0_1 \uparrow_2\rangle\right) \tag{21}$$

And likewise for the single down spin case. Particle hole symmetry implies the block with three particles (one hole) will behave the same as the one particle block with the exception of -3μ instead of $-\mu$. Finally, the half-filled with spin $S_z = 0$ block resolves into the states below. I will leave out the left hand side of the eigenvalue equation to save room.

$$= \underline{(-2\mu - U/2)}\left(|\uparrow_1\downarrow_2\rangle - |\downarrow_1\uparrow_2\rangle\right) \tag{22}$$

$$= \underline{(-2\mu + U/2)}\left(|\uparrow\downarrow_1 0_2\rangle - |0_1 \uparrow\downarrow_2\rangle\right) \tag{23}$$

$$= \underline{(-2\mu + 2\epsilon(U,t))}\left(-2t|\uparrow_1\downarrow_2\rangle - 2t|\downarrow_1\uparrow_2\rangle + (U/2 + 2\epsilon(U,t)))|\uparrow\downarrow_1 0_2\rangle + (U/2 + 2\epsilon(U,t))|0_1 \uparrow\downarrow_2\rangle\right) \tag{24}$$

$$= \underline{(-2\mu - 2\epsilon(U,t))}\left(2t|\uparrow_1\downarrow_2\rangle + 2t|\downarrow_1\uparrow_2\rangle + (-U/2 + 2\epsilon(U,t)))|\uparrow\downarrow_1 0_2\rangle + (-U/2 + 2\epsilon(U,t))|0_1 \uparrow\downarrow_2\rangle\right) \tag{25}$$

Where $\epsilon(U,t) = \sqrt{t^2 + (U/4)^2}$. I have underlined the energy eigenvalues so they stand out. The spectrum for these states is shown in Fig 4 as a function of U/t for $t = 1$ and $\mu = 0$. The lower two bands form a singlet and triplet state, where the singlet forms the non-degenerate ground state. In the large U/t limit (for $\mu = 0$) the energies of the triplet and singlet bands are

$$\text{triplet} : -U/2 \tag{26}$$

$$\text{singlet} : -2\sqrt{t^2 + (U/4)^2} \approx -U/2(1 + (4t/U)^2) = -U/2 - 4t^2/U \tag{27}$$

So, we find perturbatively that for $U/t \gg 1$ there persists a gap between the singlet ground state and the triplet band of $4t^2/U$. Within this gap is the intuition of the Mott insulator, the insulating state that arises when interactions are large enough to localize each particle on a single site to avoid the high Coulomb interaction. If every particle is confined to its own site then one might expect a 4^n-fold degeneracy for $n-$site

lattices. However, the nature of the singlet state implies if the particles are allowed to hop, then they can lose energy by hopping to a nearest neighbor and back. The amount of energy they lose during this process is $4t^2/U$. The Pauli exclusion principle states it is impossible for two fermions of the same spin to exist on the same site, therefore an arrangement of one spin per site where up spins only neighbor down spins and vice versa maximize the potential of hopping. Which in turn minimizes the energy. This leads to the characteristic anti-ferromagnetic behavior of the Mott insulator.

The energy $4t^2/U$ is the superexchange value, which turns out to be an important energy scale at $U/t \gg 1$. For example, for temperatures below the superexhange value quasi-long range anti-ferromagnetic correlations arise. [13].

The $t-J$ model is approximated from the large U/t limit where the doubly occupied sites are projected out of the state space due to large interactions, and the particle interactions from the Hubbard term are replaced with the emergent spin-spin interactions of the Heisenberg Hamiltonian with coupling constant equal to the superexchange.

$$(\text{eq.8}) \rightarrow \mathcal{H} = \mathcal{P}^{-1}\left[\mathcal{H}_{TB} + J\sum_{\langle ij\rangle}\hat{S}_i\hat{S}_j - \mu\sum_i \hat{n}_i\right]\mathcal{P} \tag{28}$$

Where the projection operator, $\mathcal{P} = 1 - \sum_i |\uparrow\downarrow_i\rangle\langle\uparrow\downarrow_i|$

4 Numerical Techniques

Calculations of the full spectrum for lattice sizes larger than about 2×2 quickly become impossible using modern computational methods. Therefore we must rely on numerical calculations for thermodynamic quantities. We employ a Determinantal Quantum Monte Carlo (DQMC) procedure for such calculations. The expectation value of some operator $\hat{A}$, involves computing [14]

$$\langle\hat{A}\rangle = Tr[\hat{A}e^{-\beta\mathcal{H}}]/Tr[e^{-\beta\mathcal{H}}] \tag{29}$$

If the tight binding and Hubbard terms commuted we could calculate each term separately: $e^{-\beta\mathcal{H}} = e^{-\beta\mathcal{H}_{TB}}e^{-\beta\mathcal{H}_H}$. Since they do not, we employ a Trotter-Suzuki decomposition to split up the quadratic and quartic terms in order to deal with the quartic terms separately.[15]

$$e^{-\beta\mathcal{H}} = \prod_l^L e^{-\Delta\tau\mathcal{H}} = \prod_l^L e^{-\Delta\tau\mathcal{H}_{TB}}e^{-\Delta\tau\mathcal{H}_H} + \mathcal{O}(\Delta\tau^2[\mathcal{H}_{TB},\mathcal{H}_H]) \tag{30}$$

This decomposition essentially maps the 2D quantum problem to a 2+1D classical problem where the lattice is allowed to evolve over the imaginary time parameter τ. The length of this dimension is set by the inverse temperature

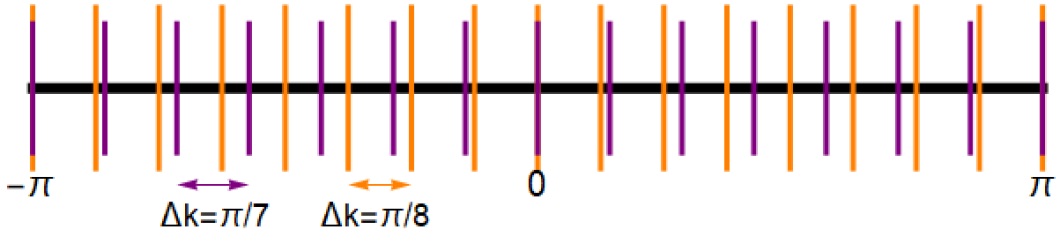

Figure 5: Momentum states for a one dimensional, 16 site chain (orange) and momentum states for a one dimensional, 14 site chain (purple) compliment each other by providing data for k-states that are inaccessible to only only one of these cluster sizes.

$$\beta = L\Delta\tau \tag{31}$$
$$\beta = 1/k_b T \tag{32}$$

Where L is the number of imaginary time steps and each step is $\Delta\tau$ in length. It is important to keep $\Delta\tau$ small so as to keep the error from the two non-commuting terms small. This process is known as quantum-classical mapping.

Finally, the Hubbard term needs to be quadratic which is possible with a Hubbard-Stratonovich transform.[16]

$$e^{-\Delta\tau U n_{\uparrow,i} n_{\downarrow,i}} = Tr_\sigma \left[exp\left(\lambda\sigma(n_{\uparrow,i} - n_{\downarrow,i}) - \frac{\Delta\tau U}{2}(n_{\uparrow,i} + n_{\downarrow,i}) \right) \right] \tag{33}$$
$$\lambda = 2\arctan\left(\sqrt{arctanh(\Delta\tau/4)}\right) \tag{34}$$

Which assigns an Ising spin $\sigma \in \{-1, 1\}$ to each site. We employ a Determinantal Quantum Monte Carlo (DQMC) which uses a metropolis algorithm to sweep through the lattice attempting to flip the Ising spins. One sweep constitutes the algorithm attempting to flip the spin on each site of the 2+1D lattice. 1000 warm up sweeps allows the system to adjust to equilibrium, while 15000 measurement sweeps are used for estimating thermodynamic quantities and errors. We set $L = 80$ and $\Delta\tau = 1/40t$, which fixes the temperature at $T = 0.5t$ *or* $\beta = 2/t$. This is 1/16 the bandwidth. The large temperature is necessary because the DQMC runs into the famous fermion sign problem which is exacerbated by small temperatures, large lattice sizes, and large values of U.

We average the results from seven trials trials to increase statistics. Four of these trials are conducted on a 16×16 cluster, three on a 14×14 cluster. The two lattice sizes compliment by providing data for k-states that are in-accessible by either lattice size individually, while affecting quantities like the density or compressibility to a negligible degree. A visual demonstration is presented in Fig 5.

5 Compressibility and Magnetic Susceptibility

The two response functions electronic compressibility and magnetic susceptibility are both useful diagnostics of phase. The measure of compressibility, κ, is zero for the Mott and band insulating phases and positive for metallic phases as shown in Fig. 9a. Experiments on cold atoms have demonstrated that kinks in the local compressibility are also useful in defining boundaries between superfluid and normal phases.[17] Meanwhile, susceptibility, χ, is large when spins are easy to flip which is the case for the spin localized Mott insulating phase, which is confirmed by our DQMC measurement of susceptibility in Fig 6 for a lattice size of 6×6 and temperature of $T = t/2$. This has also been confirmed in cold atom experiments. [13]

With the addition of a Zeeman field to our Hamiltonian, parameterized with field strength h, we can calculate κ and χ from the fluctuation dissipation theorem.

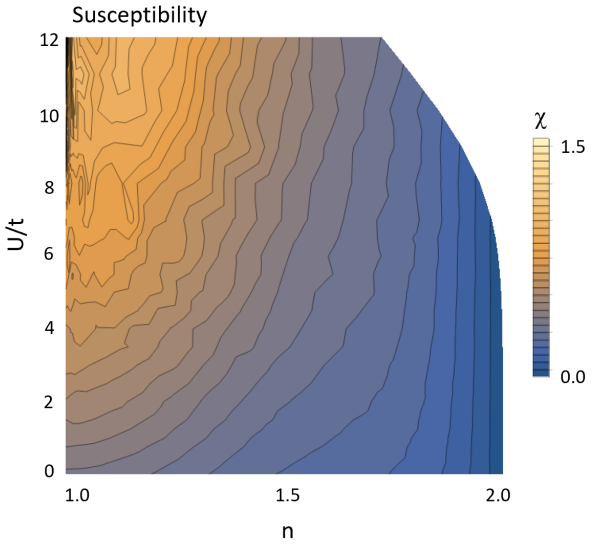

Figure 6: Magnetic susceptibility is calculated for the particle doped Fermi Hubbard model on a 6×6 lattice at zero field strength over the parameter space of density, n, and interaction potential, U, and for $T = t/2$. The magnetic susceptibility is large when particles are localized to one site and very few sites are doubly occupied, as is the case for the (n=1, $U/t \gg 1$) Mott insulator phase.

$$\kappa n^2 = \frac{1}{N_s}\frac{\partial \langle \hat{N} \rangle}{\partial \mu} = \frac{\beta}{N_s}\left(\langle \hat{N}^2 \rangle - \langle \hat{N} \rangle^2 \right) \tag{35}$$

$$\chi = \frac{1}{N_s}\frac{\partial \langle \hat{M} \rangle}{\partial h} = \frac{\beta}{N_s}\left(\langle \hat{M}^2 \rangle - \langle \hat{M} \rangle^2 \right) \tag{36}$$

Where N_s is the number of lattice sites, $\hat{N} = \sum_{i,\sigma} \hat{n}_{i,\sigma}$ is the total particle number, and $\hat{M} = \sum_i (\hat{n}_{i,\uparrow} - \hat{n}_{i,\downarrow})$ is the lattice magnetization.

The operator $\hat{N}^2$ and $\hat{M}^2$ is constructed from density-density correlation functions, $\langle \sum_{i,j} \hat{n}_i \hat{n}_j \rangle$, calculated by the DQMC.

$$\hat{N}^2 = \sum_{i,j} \langle (\hat{n}_{i,\uparrow} + \hat{n}_{i,\downarrow})(\hat{n}_{j,\uparrow} + \hat{n}_{j,\downarrow}) \rangle \tag{37}$$

$$\hat{M}^2 = \sum_{i,j} \langle (\hat{n}_{i,\uparrow} - \hat{n}_{i,\downarrow})(\hat{n}_{j,\uparrow} - \hat{n}_{j,\downarrow}) \rangle \tag{38}$$

Which are better expressed in terms of the spin correlators: $C_{\uparrow\uparrow} = \sum_{i,j} \langle \hat{n}_{i,\uparrow} \hat{n}_{j,\uparrow} \rangle$, $C_{\uparrow\downarrow} = \sum_{i,j} \langle \hat{n}_{i,\uparrow} \hat{n}_{j,\downarrow} \rangle$, and $C_{\downarrow\downarrow} = \sum_{i,j} \langle \hat{n}_{i,\downarrow} \hat{n}_{j,\downarrow} \rangle$.

$$\kappa n^2 = \frac{\beta}{N_s}\left(C_{\uparrow\uparrow} + 2C_{\uparrow\downarrow} + C_{\downarrow\downarrow} - \langle \hat{N} \rangle^2 \right) \tag{39}$$

$$\chi = \frac{\beta}{N_s}\left(C_{\uparrow\uparrow} - 2C_{\uparrow\downarrow} + C_{\downarrow\downarrow} - \langle \hat{M} \rangle^2 \right) \tag{40}$$

A curious relationship has developed between these two seemingly disparate measures of the lattice, seeing that they share several terms. Let's examine the difference of κn^2 and χ.

$$\kappa n^2 - \chi = \frac{4\beta}{N_s}\left(C_{\uparrow\downarrow} - \frac{1}{4}\langle \hat{N} \rangle^2 + \langle \hat{M} \rangle^2 \right) \tag{41}$$

$$= \frac{4\beta}{N_s}\left(\sum_{i,j} \langle \hat{n}_{i,\uparrow} \hat{n}_{j,\downarrow} \rangle - \sum_{i,j} \langle \hat{n}_{i,\uparrow} \rangle \langle \hat{n}_{j,\downarrow} \rangle \right) \tag{42}$$

As it turns out there happens to exist an unexpectedly elegant way to write this difference: the anti-aligned spin correlation function:

$$\kappa n^2 - \chi = \frac{4\beta\Delta}{N_s} \tag{43}$$

$$\Delta \equiv \sum_{i,j} \langle \hat{n}_{i,\uparrow} \hat{n}_{j,\downarrow} \rangle - \sum_{i,j} \langle \hat{n}_{i,\uparrow} \rangle \langle \hat{n}_{j,\downarrow} \rangle \tag{44}$$

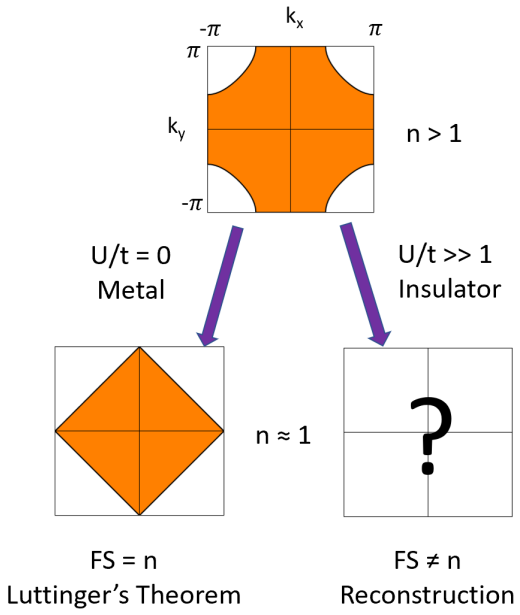

Figure 7: Luttinger's theorem, which is a statement of proportionality between the charge carrier density and the Fermi surface volume, is obeyed in a metal at any doping. When strong particle-particle interactions are introduced it is unclear how the Fermi surface transitions in the limit where $n \approx 1$.

There are three regions of the (U, t, μ) phase diagram where this correlation function is zero corresponding to an equivalence of the electronic compressibility and magnetic susceptibility. The first being the free system, $U = 0$; when the particles stop interacting, implying $\langle \hat{n}_{i,\uparrow} \hat{n}_{j,\downarrow} \rangle \to \langle \hat{n}_{i,\uparrow} \rangle \langle \hat{n}_{j,\downarrow} \rangle$ and the two terms cancel. The other two instances of $\Delta = 0$ are when the band is empty or full. This is the trivial case because the expectations for each site in equation 44 are zero and one respectively for both terms. What does this tell us about the nature of these three phases? κ and

χ are functions of the energy required to add a particle to the lattice and flip a particle's spin respectively. In the empty and full band the minimum energy required to induce a spin change requires the addition of a particle or hole, which explains the equivalence of κ and χ. The best intuition for why the non-interacting system shares this property necessitates a temperature of zero. In the $T \to 0, U \to 0$ limit the Fermi surface separates the occupied states from the unoccupied states. Spins cannot be flipped easily because for every occupied state $|\mathbf{k}, \uparrow\rangle$ there is always an occupied $|\mathbf{k}, \downarrow\rangle$. Therefore, the minimum amount of energy required to induce a spin change is the Fermi energy; which is equivalent to the energy required to add a particle to such a lattice.

6 Fermi Surface Restructuring

Luttinger's theorem is a statement of proportionality between the Fermi surface volume and the charge carrier density proven by Luttinger in the 60s.[12] Fig 7 demonstrates this proportionality for a metal. It is currently unclear how or if Luttinger's theorem is accurate for non-Fermi liquids, and for insulating states the theorem breaks down altogether due to the lack of a Fermi surface.

Our aim will be to examine the Fermi surface at large interaction strengths across the doping driven metal-insulator phase transition. We will soon see that restructuring occurs where states are being frozen due to the proximity to the Mott insulator, in seeming violation of Luttinger's theorem.

6.1 Motivation

The Fermi surface is known to restructure due to competing order such as charge density wave order (CDW), where the on-site particle density is no longer translationally invariant, but modulates periodically. This restructuring of the size of the unit cell must restructure the Fermi surface. A consequence of CDW is the breaking of particle-hole symmetry which can either be achieved in a modeled system by including a next nearest hopping term or a next nearest interaction term in the Hamiltonian, both of which fail to produce an equivalent Hamiltonian under a particle-hole transform. CDW will reconstruct the Fermi surface to form four small nodal electron like pockets.[10]

Spin density wave order (SDW) will reconstruct the Fermi surface in pockets around a Lifshitz critical point where there are many states on the Fermi surface that are exactly $k = (\pm\pi, \pm\pi)$ from another state on the Fermi surface leading to a divergence in the spin susceptibility.

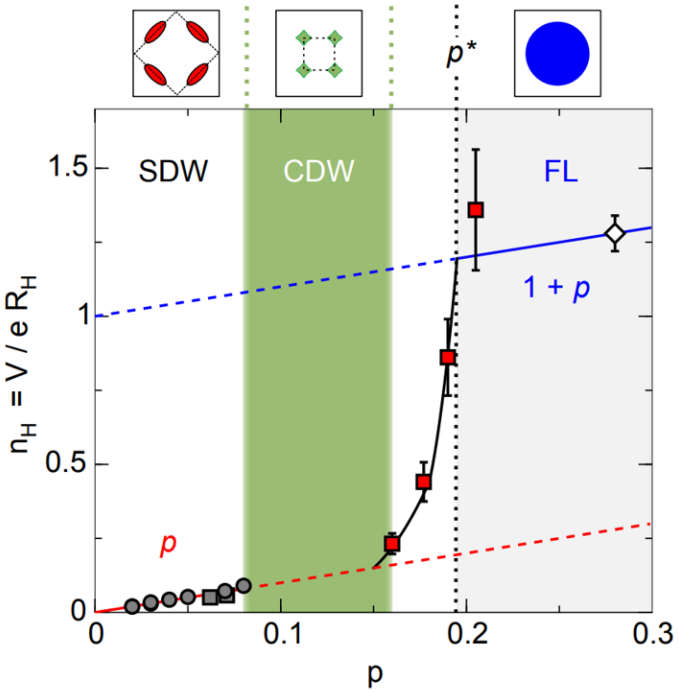

Figure 8: The Hall coefficient gives information about the density of charge carriers and thus also gives information about the size of the Fermi surface. Tallefer et al. discovered in YBCO at T = 50K that the proportionality of the Hall coefficient transitions from $1 + p$ to p at the critical doping for the pseudogap phase $p*$. Because this transition happens after the critical doping for charge density wave order, it is concluded that these two phenomena are distinct.[10]

Recently, a team discovered using Hall measurements in YBCO at T = 50K that there exists a critical doping where a transition in the proportionality of the Hall coefficient, n_H, occurs. At $p^* = 0.19$ the Hall coefficient transitions from a proportionality of $1+p$ to p, where p is the hole doping.[10] n_H gives information about the charge carrier density and by Luttinger's Theorem the size of the Fermi surface, as well. Therefore, a transition in the Hall coefficient implies Fermi surface restructuring. A figure from their Nature paper is shown in Fig. 8 which shows the transition.

The team notes that the doping range for charge density wave ordering, p^{CDW}, in YBCO are $0.08 < p < 0.16$,[18] and thus the transition is not a consequence of charge density wave ordering. Instead, the transition in the size of the Fermi surface is likely related to the elusive pseudogap phase, which begins at the critical doping $p^* = 0.19$.[19]

Our Hamiltonian does not possess charge density wave ordering capabilities due to its implicit particle-hole symmetry, therefore, if this phenomenon is in fact distinct from CDW then we may find the same phenomenon using our simple model. A question remains, however: why is the size of the Fermi surface changing from enclosing $1+p$ holes to only p holes? We believe the transition can be rudimentarily explained by the formation of a "Mott background" or a background of "Mott sites" where one particle per site remains frozen due to strong particle-particle interactions. In this interpretation, one particle per site forms the background lattice and does not carry charge freely through the lattice, which changes the charge carrier density from $1+p$ to p. Why are the remaining p particles not frozen with the others? Particles hopping on the Mott background are unencumbered by particle-particle interactions because every site has a particle on it. A particle cannot avoid the energy cost of U and therefore is effectively free of particle-particle interactions. A useful way to think about charge transport on a Mott background is to imagine the doubly occupied sites (or in the context of doped holes, the empty sites) "hopping" from one site to the next. Effectively the doublons (or empty sites) have become the charge carriers.

6.2 Fermi Surface

The formation of Mott sites should suppress the compressibility, $\kappa(U, \mu, T)$, of the lattice because these background particles are frozen and hence incompressible. We take a cut of constant interaction potential ($U/t = 10$ seen in Fig. 9a) where the strong suppression of κ is due to the formation of these Mott sites and the opening of a gap in the spectrum.

The agreement between the numerical derivative, $\frac{\Delta n}{\Delta \mu}$ and the fluctuation dissipation theorem calculation in Fig 9(b) serves as a non-trivial check of our numerics. At a fixed interaction strength, a Mott insulator to metal transition is driven by doping the lattice.

To support the claim that this suppression of the compressibility can be explained by the formation of the Mott background, where the charge carriers are essentially the doublons or holes depending on whether the density is higher than unity or lower, we compare the compressibility of a non-interacting system ($U/t = 0$)

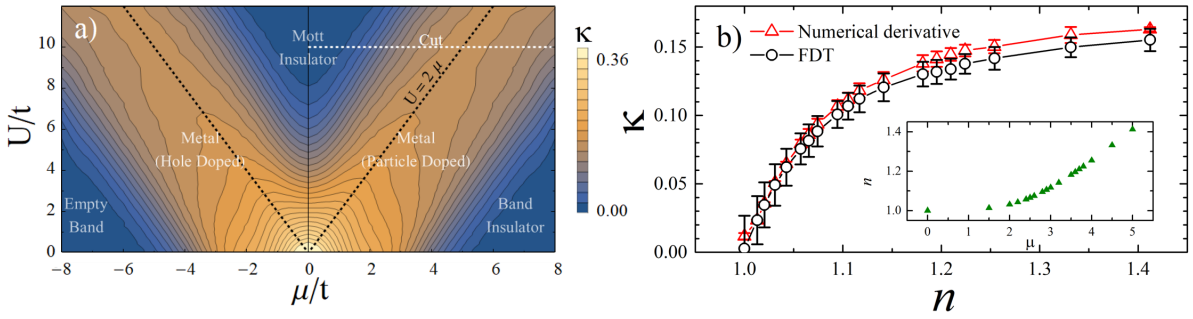

Figure 9: a) Compressibility κ is calculated on a 6 × 6 lattice as a function of interaction potential (U) and chemical potential (μ) at $\beta t = 2$. Small (close to zero) compressibility (blue) indicates Mott and band insulating phases; positive compressibility corresponds to a metallic phase. b) Compressibility κ is calculated for a 16 × 16 system with a fixed interaction strength ($U = 10t$) and varying density/ chemical potential (μ) for $\beta t = 2$.

with a highly interacting system ($U/t = 7$) in Fig 10. The density of doublons (or holes), which is taken to be the density of charge carriers is $p = |n - 1|$. Using this assumption, we notice that for large interaction strengths, around half filling the compressibility is suppressed due to a lack of charge carrying doublons or holes and the system becomes a Mott insulator, which corresponds to an empty band in the context of the Mott background. For fillings close to 2, the compressibility should approach zero for both cases as the band is being filled in both cases.

Another non-trivial check of our assumption is that the compressibility of the strongly-interacting system at $n = 1 + p = 1.5$ should be approximately half the compressibility of the non-interacting system at $n = 1$:

$$\kappa(U/t \gg 1, p = 0.5) \approx \frac{1}{2}\kappa(U/t = 0, p = 0) \tag{45}$$

This is because the approximate density of charge carriers in the non-interacting case at $n = 1$ is twice the approximate density of charge carriers in the strongly-interacting case at $n = 1.5 (p = 0.5)$. This is also supported by Fig 10. The qualitative similarities of the non-interacting compressibility over the density intervals of $0 < n < 2$ compared to twice the compressibility of the interacting system over the density intervals of $1 < n < 2$ strongly suggests that a Mott background is a useful picture with which to understand the suppression of the compressibility in the Mott limit.

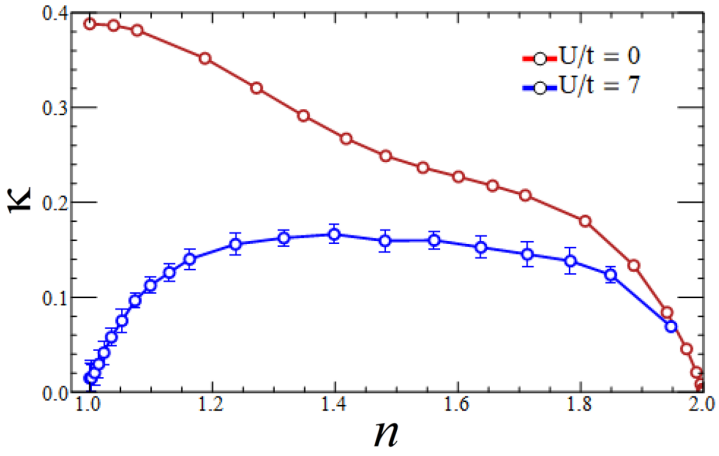

Figure 10: Compressibility is calculated for a 6×6 cluster size for a non-interacting metal and a strongly interacting system at $T = t/2$ as a function of density. The compressibility of the non-interacting system over the interval $1 < n < 2$ is qualitatively similar to twice the compressibility of the strongly interacting system over the interval $1.5 < n < 2$.

Now that we have shown how the Mott background explains the suppression of compressibility in the Mott limit and vice versa, we aim to show how the it restructures the Fermi surface. Using the DQMC, we directly calculate the Green's function in imaginary time, τ, and use a maximum entropy analytic continuation procedure to obtain the spectral function from the integral expression

$$G_{\mathbf{k}}(\tau) = \int_{-\infty}^{\infty} \frac{e^{-\omega\tau}}{1 + e^{-\beta\omega}} A(\mathbf{k}, \omega) d\omega \tag{46}$$

The spectral function, $A(\mathbf{k}, \omega) = -(1/\pi)\mathrm{Im}G^{ret}_{\mathbf{k}}(\omega)$, gives information about the probability of finding a particle in a state $(\mathbf{k}, \omega)$. Particles on the Fermi surface have large spectral weights at $\omega = 0$ because for states on the Fermi surface no energy is required to excite it to the next free state. We construct one interpretation of the Fermi surface as the locus of k-states where $A(\mathbf{k}, \omega = 0)$ is large.

A related quantity is the retarded Green's function

$$G^{ret}_{\mathbf{k}}(E) = \mathcal{P} \int_{-\infty}^{\infty} d\omega \frac{A(\mathbf{k}, \omega)}{\omega - E} \tag{47}$$

Where $\mathcal{P}$ is the principle part. The retarded Green's function provides another interpretation of the Fermi surface as the boundary over the Brillouin zone $G^{ret}_{\mathbf{k}}(E = 0) = 0$ marks the boundary in k-space where the sign changes due to a divergence which marks the Fermi surface.[20]

The last Fermi surface diagnostic that we use is the momentum distribution function (MDF)

$$n_{\mathbf{k}} = 1/2 \tag{48}$$

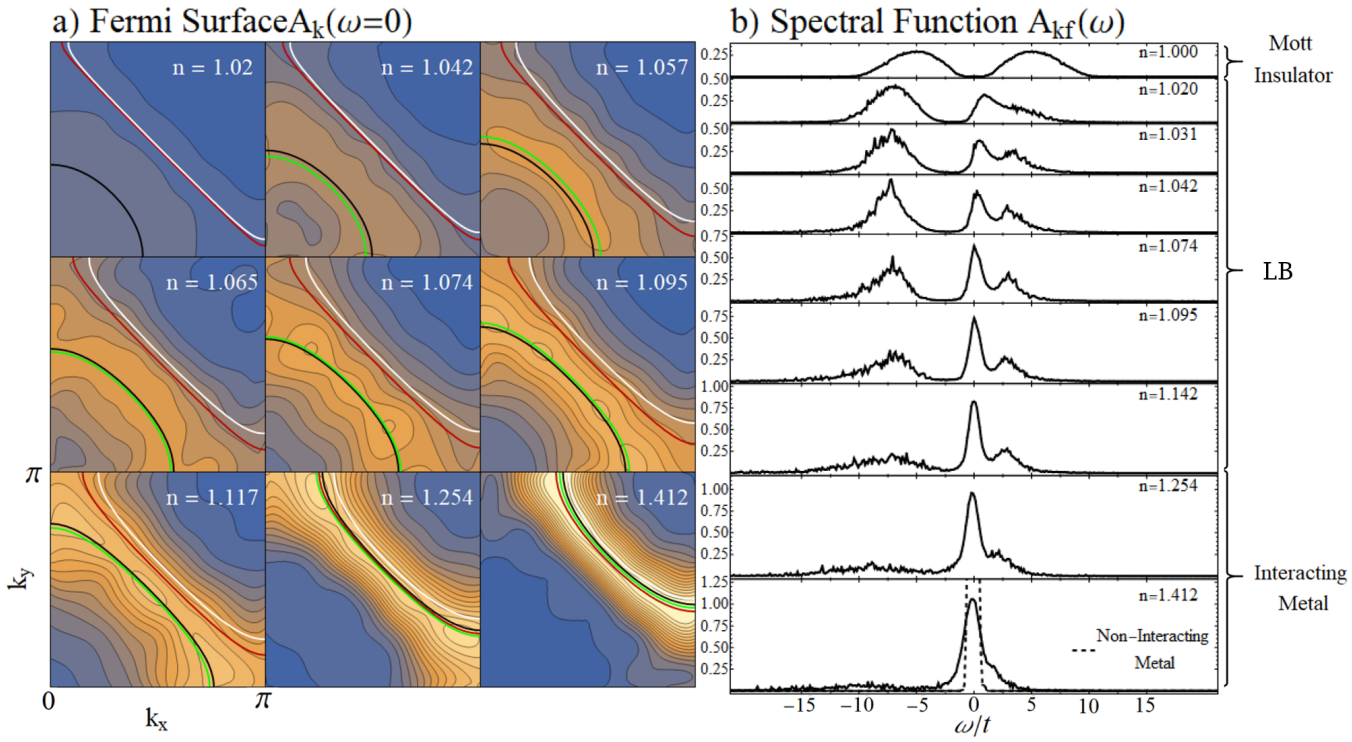

Figure 11: a) The spectral weight, $A(\mathbf{k}, \omega = 0)$, in the Brillouin zone for a 16×16 site square lattice. We show different interpretations of the Fermi surface as contours. We have set interaction potential $U = 10t$ and $\beta t = 2$. Non-interacting Fermi surface(white); Momentum distribution function (MDF): the contour formed by $n_{\mathbf{k}} = 1/2$ (red); locus of spectral weight at $A(\mathbf{k}, \omega = 0)$ (black); and retarded Green's function: $G^{ret}_{\mathbf{k}}(E = 0) = 0$ (green). b) $A(\mathbf{k}, \omega)$ averaged over all k-states weighted by the value of $A(\mathbf{k}, \omega = 0)$ so to extrapolate the spectral function of the Fermi momentum. Total spectral weight is constant: $\frac{1}{\pi}\int_{-\infty}^{\infty} A(\mathbf{k}, \omega) d\omega = 1$. Finite size effects naturally broaden the spectral function. The non-interacting metal spectral function at the same temperature (dashed) is contrasted with the interacting metal for $n = 1.412$. Where the non-interacting Fermi surface and spectral contours do not agree we have labeled LB for Luttinger's rule breaking.

In the thermodynamic limit for a non-interacting system at $T = 0$, the MDF has a jump of size unity $Z = 1$ at the Fermi wave vector, $\mathbf{k}_f$, when the system transitions from occupied states below k_F to zero occupancy above. In a Fermi liquid, following Luttinger's theorem, $\mathbf{k}_f$ does not change and $0 < Z \leq 1$. Due to inter-electron interactions, some of the states below $\mathbf{k}_f$ are scattered into states above but nevertheless in a Fermi liquid, a finite step at $\mathbf{k}_f$ persists at $T = 0$. At finite T, naturally the step gets rounded; however, the boundary where $n_{\mathbf{k}} = 1/2$ can still extract the location of the underlying Fermi surface.

Fig 11a shows for different densities the spectral weight $A(\mathbf{k}, \omega = 0)$ over the Brillouin zone. The black contour is the locus of spectral weight, or in other words where the boundary would likely be in the limit of $T \to 0$. The green contour shows where the boundary of the Green's function $G^{ret}_{\mathbf{k}}(E = 0) = 0$ lies, and the red boundary shows where $n_{\mathbf{k}} = 1/2$. For reference we included the non-interacting Fermi surface that is proportional to the density for all dopings; this is the white curve.

For dopings greater than $p \gtrsim 0.2$ each of these metrics show stark qualitative agreement, especially considering the errors inherent to the DQMC. Below dopings $p \lesssim 0.2$, however the locus of spectral weight (black) and the Green's function boundary (green) depart from the MDF (red) and non-interacting Fermi surface (white). At smaller dopings still, the momentum distribution function still remains in agreement (within uncertainty) with the non-interacting Fermi surface. This is evidence that in the regime below $p \lesssim 0.2$ the system is not a Fermi liquid because the MDF metric, which always gives the Fermi surface for Fermi liquids, is not agreeing with more useful interpretations of the Fermi surface like the Green's function sign change. We dub the phase where the Fermi surface does not agree with the non-interacting Fermi surface the Luttinger's rule breaking (LB) phase.

The size of the Fermi surface (black and green contours) monotonically decrease with the decreasing

momentum until the all spectral weight is destroyed in the Mott limit, where all the particles are frozen on site. This is our key result since it shows clear Fermi surface restructuring, even in the simplest version of the Hubbard model (which disregards next-nearest neighbor hopping and next-nearest neighbor particle-particle interaction) and for as high a temperature as $T = t/2$. As the doping drives the phase from metal to Mott insulator it is clear that less particles are being counted by the Fermi surface, and it is restructuring to form a boundary that encloses closer to p states than $p + 1$ states. As we saw in the case of compressibility these particles are being frozen as they form the background of Mott sites. It still is not clear why the Mott background starts to play a role for dopings close to $p \lesssim 0.2$, since in this explanation the only driving force behind the formation of the Mott background is the strong interaction and not the specific particle doping. This reveals that the "Mott background" is only a rudimentary explanation and is in no way the full picture.

FSR in the 2D Fermi-Hubbard model is strongly correlated with the pseudogap phase since both are present for doping less than. $p < 0.2$[21]

6.3 Spectral Function

In Fig 11 b we plot the spectral function as a function of ω averaged over all the momentum states in the Brillouin zone, statistically weighted by the spectral weight at $A(\mathbf{k}, \omega = 0)$.

$$A(kf, \omega) = \frac{\sum_{\mathbf{k}} A_{\mathbf{k}}(\omega) A(\mathbf{k}, \omega = 0)}{\sum_{\mathbf{k}} A(\mathbf{k}, \omega = 0)} \quad (49)$$

Although seemingly arbitrary, we construct the spectral function at the Fermi wave vector this way because of its relevance in the non-interacting/ thermodynamic limit which exactly gives the spectral function at $\mathbf{k}_f$. Note this washes out all momentum dependence of the spectral function for states on the Fermi surface; the purpose of the function $A(kf, \omega)$ is to see the qualitative distribution of states on the Fermi surface.

The interacting system shows the development of incoherent side bands or Mott bands around the peaked spectral function at $\omega = 0$. The Fermi surface restructuring is already visible below $n \approx 1.2$ and the deviation of the actual Fermi contour from the Luttinger contour only gets more pronounced as the incoherent weight increases upon approaching the Mott transition at $n = 1$. We note that the spectral gap for the Mott insulator agrees with our understanding of the Mott gap: that its magnitude is on the order of U.

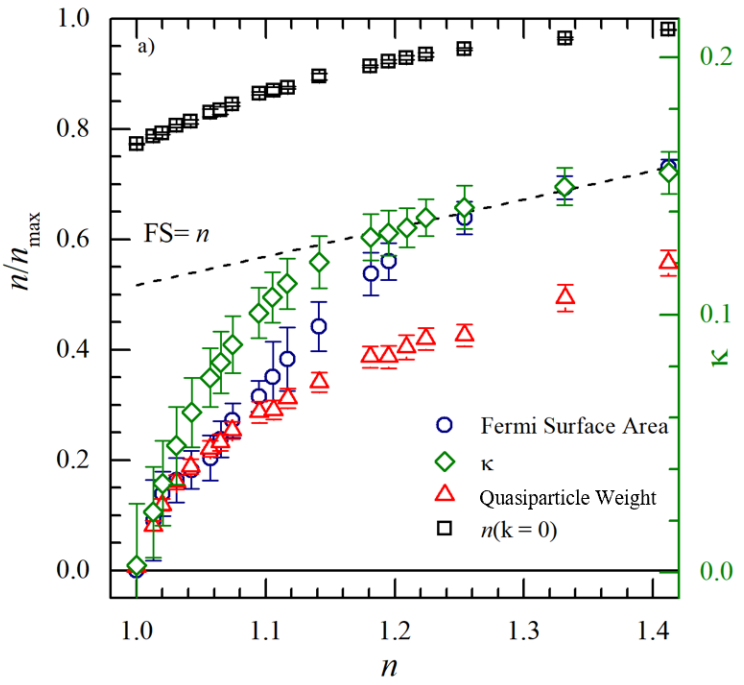

Figure 12: We calculate the number of particles enclosed by the locus of spectral weight (black) Fermi surface in Fig 11a, the occupation of the $n_{\mathbf{k}=(0,0)}$ state, and the quasiparticle weight, defined in equation 50. The area of the Fermi surface, according to Luttinger's theorem, is proportional to the density. Turning on strong interactions decreases the size of the Fermi surface for doping around 0, contradicting this rule.

The quasiparticle weight, QW, is a metric we define to help identify how the doping driven transition is affecting the spectral function. It measures the amount of spectral weight within ϵ of the origin, where ϵ is defined by the non-interacting spectral function (shown as a dashed line in the bottom panel of Fig 11b).

$$QW = \frac{1}{\pi} \int_{-\epsilon}^{\epsilon} A(kf, \omega) d\omega \quad (50)$$

In the non-interacting limit the spectral function is a delta function at $E(\mathbf{k})$, however finite size effects require a broadening of the spectral function into a Lorentzian. The quasiparticle weight is plotted in Fig 12.

Another metric we employ is the density $n_{\mathbf{k}=(0,0)}$ because this state requires the largest amount of energy to scatter to an unoccupied state. For $U = 0$, the $\mathbf{k} = (0, 0)$ state is always filled, which allows us to use $n_{\mathbf{k}=(0,0)}$ at large interaction strengths to analyze how the interaction is scattering low energy/ submerged states.

6.4 Green's Function

The contour produced by the Green's function construction and the spectral weight construction remarkably agree for the densities shown in figure 11a. We are cautious to claim that the Fermi surfaces produced by these two methods are unique and distinct interpretations of the Fermi surface, however, since both contours are essentially products of the same spectral function. Let's examine the properties of the Green's function and its usefulness.

In Luttinger's original paper, he uses the Green's function to show that the Fermi surface always encloses the proper number of particles.[12] Specifically, where the Green's function changes sign denotes the location of the Fermi surface in the Brillouin zone. In the zero temperature limit the sign of the Green's function for a state on the Fermi surface diverges at $E = 0$. $G_{\mathbf{k}}(E)$ goes through a pole, signifying the presence of a quasiparticle at the Fermi surface.

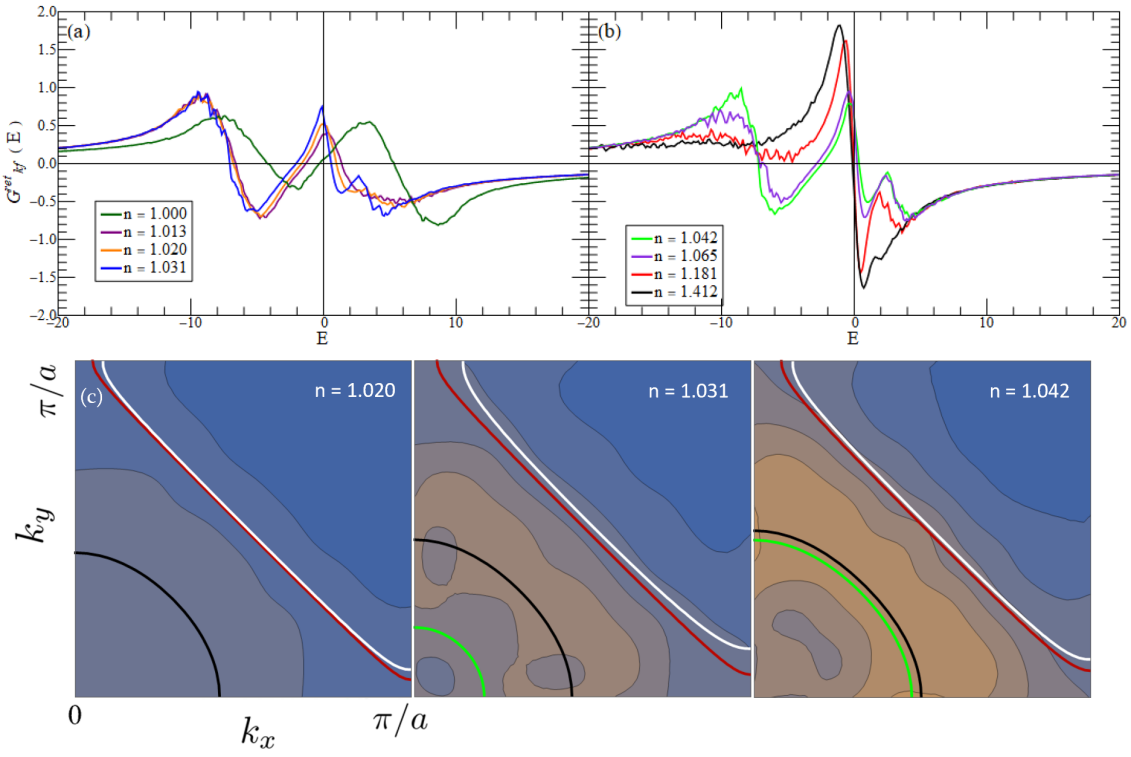

Figure 13: The retarded Greens function is calculated using equation 47 for the composite spectral function $A_{kf}(\omega)$ shown in Fig 11b. a) Small densities show a zero-like crossing of x-axis by the Green's function while b) larger densities show a pole-like crossing of the Green's function, where the smoothing of the divergence at $E = 0$ results in the crossing of the x-axis, indicative of a quasiparticle on the Fermi surface. c) For a range of intermediate densities the Green's function at kf peaks, instead of changing sign, at $E = 0$ as the pole-like sign change transitions to a zero-like sign change. This corresponds to a disagreement in the Fermi surfaces produced by the locus of spectral weight and the Green's function sign change over the Brillouin zone.

For finite temperature, however, the Green's function becomes rounded and the pole becomes a continuous function that passes through the origin at $E = 0$. We use this to construct the Green's function contour as discussed above.

This construction of the Fermi surface breaks down when zeros are present in the Green's function that are not pole-like.[22] In the case of these zeroes, the sign changes without passing through a pole which leads to a break down of Luttinger's theorem. We must, then, take great care such that we do not construct the Fermi surface using a zero like sign change of the Green's function rather than a "zero surface." This is why we do not show the Green's function contour for the density $n = 1.020$ in Fig 11. We will see what the zero surface looks like later.

For now, let's examine Fig 13a and b where we plot $G^{ret}_{kf}(E)$ for the average spectral function over the Fermi surface, $A(kf, \omega)$, given in equation 49. A good check that $A(kf, \omega)$ is an accurate representation of an average spectral function over the Fermi surface is that $G^{ret}_{kf}(E = 0) = 0$. If this condition holds (as it does for $n \gtrsim 1.042$ in Fig 13b), then $G^{ret}_{kf}(E)$ represents an average of the Greens function over the Fermi surface. The curve for the metallic phase ($n = 1.412$) depicts a pole-like sign change due to its large quasiparticle weight at $\omega = 0$. As spectral weight is shifted to the incoherent Mott lobes the pole-like sign change becomes less pronounced, but remains pole-like.

On the other side of the phase transition, the Mott insulator Green's function ($n = 1.000$) changes sign three times and does not pass the x-axis in a manner characteristic of a pole-like sign change. The lack of quasiparticle weight in the Mott limit guarantees this. For the densities $1.000 < n < 1.042$ we note the transition of a pole-like sign change to zero-like. During this transition the Green's function at kf peaks at $E = 0$ instead of changing sign, implying that the Fermi surface constructed via the spectral function no longer agrees with the Fermi surface constructed via the retarded Green's function. Fig 13c shows that for densities less than $n < 1.042$ the two constructed Fermi surfaces do not agree, and for $n \lesssim 1.020$ the Fermi surface completely disappears using the Green's function diagnostic.

We note that for the metallic phase that does not break Luttinger's counting rule the Green's function for kf crosses the x-axis once at $E = 0$ pole-like, while the Mott insulating phase possesses three zeros, each zero-like, and for the Luttinger Breaking (LB) phase (specifically $1.031 < n \lesssim 1.200$) there are two zero-like sign changes and one pole-like sign change at $E = 0$. It is unclear, however, if this property can be thought of as characteristic of the LB phase or if it is merely coincidental.

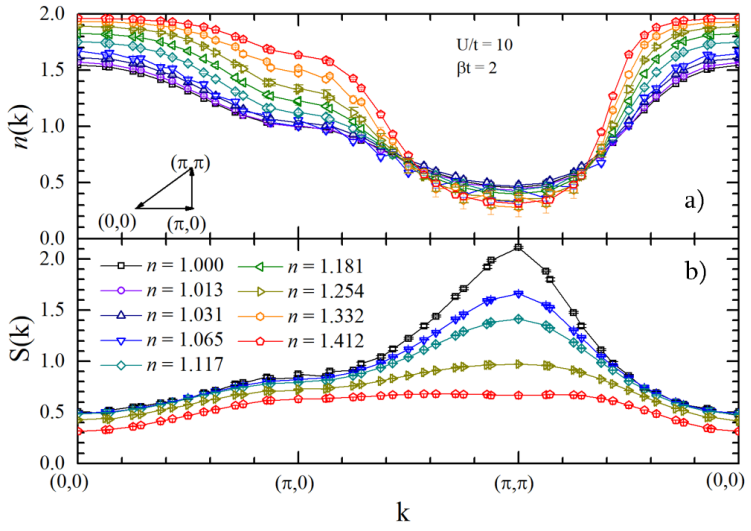

Figure 14: a) The momentum distribution function (MDF) is plotted for multiple values of n on a path taken across the Brillouin zone. b) Spin Spin correlations across the Brillouin zone show spin ordering in the Mott limit and the highly interacting metallic limit.

6.5 Order Driven Fermi Surface Restructuring

Reconstruction of the Fermi surface is driven by some arising order such as spin density wave[23], charge density wave[24], or the presence of superconductivity. What competing order is driving the restructuring of the Fermi surface? Superconducting order can immediately be ruled out because of the temperature. Similarly CDW cannot be the order in question because our particle-hole symmetric Hamiltonian does not break translational symmetry. In other words, the structure factor

$$S_{\mathbf{k}} = \sum_{\mathbf{i},\mathbf{j}} \langle \hat{n}_{\mathbf{i}} \hat{n}_{\mathbf{j}} \rangle e^{i(\mathbf{i}-\mathbf{j})\cdot\mathbf{k}} \tag{51}$$

is only statistically greater than zero when $\mathbf{k} = (0, 0)$. This leaves the possibility for spin density wave order to be the culprit, however, our results are inconsistent with predictions of SDW order which claim a divergence in the susceptibility and a Fermi surface that forms pockets on the border of the non-interacting Fermi surface.[25] Also, if SDW is the restructuring order then we expect to see a sharp peak in the spin structure factor, while Fig 14c shows a broad peak starting to form when $p = 0$. This peak is strongly suppressed by doping, effectively ruling out SDW.

7 Conclusion

Our results suggest that if secondary ordering in the spin, charge or pairing channel is suppressed, the proximity to a Mott insulator alone drives the reconstruction of the Fermi surface. Studies have found similar violations of Luttinger's theorem for large temperatures using the related t-J model.[26] Although, we do not currently understand the order by which the Fermi surface is restructuring, calculations imply a topological nature from the winding number of the single-particle Green's function.[27] Also, topological order in the pseudogap phase of the Fermi-Hubbard model may drive a breaking of Luttinger's theorem.[28, 29, 30] This theoretical topologically ordered phase possesses a Fermi surface composed of fractionalized spinons and is dubbed FL*.[31] Such an FL* phase with a reconstructed Fermi surface could be a possible description of the pseudogap phase.[32] Our results on the Hubbard model are the first indication of such an FL* phase from a controlled calculation with only statistical errors.

Here we showed that Fermi surface restructuring can occur in the very simplest version of the Fermi-Hubbard model, however going forward it is necessary to study this transition with next nearest neighbor hopping for a more realistic model of cuprates. Although, we find that the the Fermi surface in our model restructures at approximately the same doping as in YBCO[10] and they both restructure to form a smaller Fermi surface, there are some glaring differences that have yet to be explained. The most obvious is that the model's Fermi surface does not restructure to enclose a number of states proportional to p rather than $1 + p$; yet another indictment on the "Mott background" explanation. This could be because of the high temperature our model is simulated at or because of competing order effects in YBCO. Therefore, the temperature dependence of the transition is something that must be examined closely. Furthermore, a realization of FSR found in the LB phase in cold atom experiments may provide conclusive evidence linking the pseudogap phase and the LB phase.

Currently, we are trying to ameliorate the sign problem in our simulations which prevents access to statistically sound data for temperatures less than about $t/2$ for this system size. We are also attempting to pioneer a machine learning technique for retrieving the centrally important spectral function from the Green's function. This will reduce the hidden error associated with the maximum entropy method we used to construct the spectral funciton.

References

[1] Louis Taillefer. Fermi surface reconstruction in high-tcsuperconductors. *Journal of Physics: Condensed Matter*, 21(16):164212, mar 2009.

[2] P. W. ANDERSON. The resonating valence bond state in la2cuo4 and superconductivity. *Science*, 235(4793):1196–1198, 1987.

[3] Russell A. Hart, Pedro M. Duarte, Tsung-Lin Yang, Xinxing Liu, Thereza Paiva, Ehsan Khatami, Richard T. Scalettar, Nandini Trivedi, David A. Huse, and Randall G. Hulet. Observation of antiferromagnetic correlations in the Hubbard model with ultracold atoms. *Nature*, 519, 2015.

[4] Peter T. Brown, Debayan Mitra, Elmer Guardado-Sanchez, Peter Schauß, Stanimir S. Kondov, Ehsan Khatami, Thereza Paiva, Nandini Trivedi, David A. Huse, and Waseem S. Bakr. Spin-imbalance in a 2d fermi-hubbard system. *Science*, 357(6358):1385–1388, Sep 2017.

[5] Elliott H. Lieb and F. Y. Wu. Absence of mott transition in an exact solution of the short-range, one-band model in one dimension. *Phys. Rev. Lett.*, 20:1445–1448, Jun 1968.

[6] P W Anderson, P A Lee, M Randeria, T M Rice, N Trivedi, and F C Zhang. The physics behind high-temperature superconducting cuprates: the plain vanilla version of RVB. *Journal of Physics: Condensed Matter*, 16(24):R755–R769, jun 2004.

[7] Arun Paramekanti, Mohit Randeria, and Nandini Trivedi. Projected wave functions and high temperature superconductivity. *Phys. Rev. Lett.*, 87:217002, Nov 2001.

[8] Claudius Gros. Physics of projected wavefunctions. *Annals of Physics*, 189(1):53 – 88, 1989.

[9] Tom Timusk and Bryan Statt. The pseudogap in high-temperature superconductors: an experimental survey. *Reports on Progress in Physics*, 62(1):61–122, jan 1999.

[10] S. Badoux, W. Tabis, F. Laliberté, G. Grissonnanche, B. Vignolle, D. Vignolles, J. Béard, D. A. Bonn, W. N. Hardy, R. Liang, N. Doiron-Leyraud, Louis Taillefer, and Cyril Proust. Change of carrier density at the pseudogap critical point of a cuprate superconductor. *Nature*, 531:210–214, 2016.

[11] Junfeng He, Costel R. Rotundu, Mathias S. Scheurer, Yu He, Makoto Hashimoto, Ke-Jun Xu, Yao Wang, Edwin W. Huang, Tao Jia, Sudi Chen, Brian Moritz, Donghui Lu, Young S. Lee, Thomas P. Devereaux, and Zhi-xun Shen. Fermi surface reconstruction in electron-doped cuprates without antiferromagnetic long-range order. *Proceedings of the National Academy of Sciences*, 116(9):3449–3453, 2019.

[12] J. M. Luttinger. Fermi surface and some simple equilibrium properties of a system of interacting fermions. *Phys. Rev.*, 119:1153–1163, Aug 1960.

[13] Lawrence W. Cheuk, Matthew A. Nichols, Katherine R. Lawrence, Melih Okan, Hao Zhang, Ehsan Khatami, Nandini Trivedi, Thereza Paiva, Marcos Rigol, and Martin W. Zwierlein. Observation of spatial charge and spin correlations in the 2d fermi-hubbard model. *Science*, 353(6305):1260–1264, 2016.

[14] R. Blankenbecler, D. J. Scalapino, and R. L. Sugar. Monte Carlo calculations of coupled boson-fermion systems. I. *Physical Review D*, 24:2278, 1981.

[15] Masuo Suzuki. Relationship between d-Dimensional Quantal Spin Systems and (d+1)-Dimensional Ising Systems: Equivalence, Critical Exponents and Systematic Approximants of the Partition Function and Spin Correlations. *Progress of Theoretical Physics*, 56(5):1454–1469, 11 1976.

[16] J. E. Hirsch. Two-dimensional hubbard model: Numerical simulation study. *Phys. Rev. B*, 31:4403–4419, Apr 1985.

[17] Qi Zhou, Yasuyuki Kato, Naoki Kawashima, and Nandini Trivedi. Direct mapping of the finite temperature phase diagram of strongly correlated quantum models. *Phys. Rev. Lett.*, 103:085701, Aug 2009.

[18] S. Blanco-Canosa, A. Frano, E. Schierle, J. Porras, T. Loew, M. Minola, M. Bluschke, E. Weschke, B. Keimer, and M. Le Tacon. Resonant x-ray scattering study of charge-density wave correlations in $yba_2cu_3o_{6+x}$. *Phys. Rev. B*, 90:054513, Aug 2014.

[19] J.L. Tallon and J.W. Loram. The doping dependence of t* – what is the real high-tc phase diagram? *Physica C: Superconductivity*, 349(1):53 – 68, 2001.

[20] Rajdeep Sensarma, Mohit Randeria, and Nandini Trivedi. Can one determine the underlying fermi surface in the superconducting state of strongly correlated systems? *Phys. Rev. Lett.*, 98:027004, Jan 2007.

[21] M Jarrell, Th Maier, M. H Hettler, and A. N Tahvildarzadeh. Phase diagram of the hubbard model: Beyond the dynamical mean field. *Europhysics Letters (EPL)*, 56(4):563–569, nov 2001.

[22] Kiaran B. Dave, Philip W. Phillips, and Charles L. Kane. Absence of luttinger's theorem due to zeros in the single-particle green function. *Phys. Rev. Lett.*, 110:090403, Feb 2013.

[23] Suchitra E. Sebastian, N. Harrison, C. H Mielke, Ruixing Liang, D. A. Bonn, W. N. Hardy, and G. G. Lonzarich. Spin-order driven fermi surface reconstruction revealed by quantum oscillations in an underdoped high T_c superconductor. *Phys. Rev. Lett.*, 103:256405, Dec 2009.

[24] Yuval Gannot, B. J. Ramshaw, and Steven A. Kivelson. Fermi surface reconstruction by a charge density wave with finite correlation length. *Phys. Rev. B*, 100:045128, Jul 2019.

[25] David LeBoeuf, Nicolas Doiron-Leyraud, B. Vignolle, Mike Sutherland, B. J. Ramshaw, J. Levallois, R. Daou, Francis Laliberté, Olivier Cyr-Choinière, Johan Chang, Y. J. Jo, L. Balicas, Ruixing Liang, D. A. Bonn, W. N. Hardy, Cyril Proust, and Louis Taillefer. Lifshitz critical point in the cuprate superconductor $\mathrm{yba_2cu_3o_y}$ from high-field hall effect measurements. *Phys. Rev. B*, 83:054506, Feb 2011.

[26] W. O. Putikka, M. U. Luchini, and R. R. P. Singh. Violation of luttinger's theorem in the two-dimensional t- J model. *Phys. Rev. Lett.*, 81:2966–2969, Oct 1998.

[27] Kazuhiro Seki and Seiji Yunoki. Topological interpretation of the luttinger theorem. *Phys. Rev. B*, 96:085124, Aug 2017.

[28] Mathias S. Scheurer, Shubhayu Chatterjee, Wei Wu, Michel Ferrero, Antoine Georges, and Subir Sachdev. Topological order in the pseudogap metal. *Proceedings of the National Academy of Sciences*, 115(16):E3665–E3672, 2018.

[29] Subir Sachdev. Topological order, emergent gauge fields, and fermi surface reconstruction. *Reports on Progress in Physics*, 82(1):014001, nov 2018.

[30] Shiro Sakai, Yukitoshi Motome, and Masatoshi Imada. Evolution of electronic structure of doped mott insulators: Reconstruction of poles and zeros of green's function. *Phys. Rev. Lett.*, 102:056404, Feb 2009.

[31] T. Senthil, Subir Sachdev, and Matthias Vojta. Fractionalized fermi liquids. *Phys. Rev. Lett.*, 90:216403, May 2003.

[32] Wei Wu, Mathias S. Scheurer, Shubhayu Chatterjee, Subir Sachdev, Antoine Georges, and Michel Ferrero. Pseudogap and fermi-surface topology in the two-dimensional hubbard model. *Physical Review X*, 8(2), May 2018.